

PHY 338k Lab Report 1

Lily Nguyen with Anna Grove

September 18, 2025

1 Introduction

2 Lab 1: Basic measurements and oscilloscope use

2.1 Wiring inside the breadboard

Using a digital multimeter in continuity mode, we tested the internal connections of the breadboard. Figure 1 shows a diagram of the wiring.

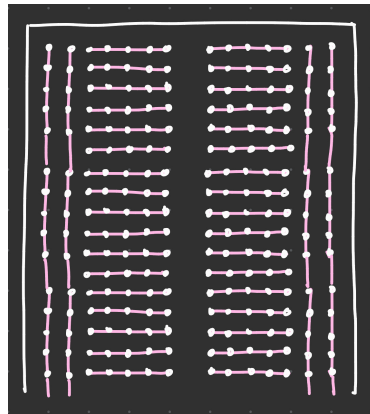


Figure 1: Schematic of the internal wiring of the breadboard.

2.2 Output impedance

2.2.1 Open circuit voltage

With the circuit setup as in Figure 1-7, we set $V_{in} = +5V$ and measured the open circuit output voltage. Using the DMM in DC mode, we got $V_{open} = 6.42V$.

2.2.2 Closed circuit current

With the circuit set up as in Figure 1-8, we measured the short circuit output current by placing the DMM in series between V_{out} and GND. We measured the short current as $I_{\text{short}} = 0.61\text{mA}$.

2.2.3 Output impedance

Using our measured open circuit voltage short circuit current, we calculated the output impedance of the circuit as:

$$Z_{\text{out}} = \frac{V_{\text{open}}}{I_{\text{short}}} \approx 10.5\text{k}\Omega. \quad (1)$$

This value is consistent with the resistance from the circuit setup. For resistor-only circuits, the output impedance is just the total resistance value.

2.3 Voltage divider

2.3.1 Voltage divider circuit

Next, we constructed the voltage divider circuit shown in Figure 1-9 using $V_{\text{in}} = +5\text{V}$. Using the voltage divider formula, we calculated:

$$V_{\text{out}} = V_{\text{in}} \frac{R_2}{R + 1 + R_2} = 5 \cdot \frac{9.93\Omega}{9.93\Omega + 9.93\Omega} = 2.50\text{V}. \quad (2)$$

Our measured value for V_{out} was 3.207V . While it differs from the theoretical prediction by about 0.71V , it is within the correct order of magnitude, and the discrepancy is likely due to experimental error or limitations in the resistor tolerance.

2.3.2 General case voltage divider

For the general case, the voltage divider output is given by:

$$V_{\text{out}} = V_{\text{in}} \frac{R_2}{R_1 + R_2}. \quad (3)$$

In the limit that $R_2 \gg R_1$, V_{out} approaches V_{in} , meaning almost all the input voltage drops across R_2 . In the opposing limit, $R_2 \ll R_1$, V_{out} approaches zero, meaning nearly all the voltage drops across R_1 . In a physical context, when R_2 is very large, it behaves almost like an open circuit, causing almost all the voltage to drop across it. On the other hand, when R_2 is very small, it acts like a short to ground, causing the output voltage to go to zero. Note, if R_1 and R_2 are equal, the output voltage would be exactly half the input voltage.

2.4 Measuring voltage waveforms with an oscilloscope

2.4.1 Measuring the waveform from a function generator

Nest, we connected the function generator output to CH1 of the oscilloscope and set it to produce a 1kHz sine wave. We attached the 50Ω terminator at the scope input and measured the frequency as $f = 1.043\text{kHz}$ and the peak-to-peak voltage as 0.692V . Without the terminator, we measured the frequency as $f = 1.045\text{kHz}$ and the peak-to-peak voltage as $V = 1.384\text{V}$.

The waveforms we observed with and without the 50Ω terminator are shown in Figure 2. The amplitude decreased by roughly half with the terminator connected because the function generator has an internal output impedance of 50Ω . Thus, when we connect a matching 50Ω load, the circuit forms a voltage divider, which causes the output voltage to drop across both resistances equally.

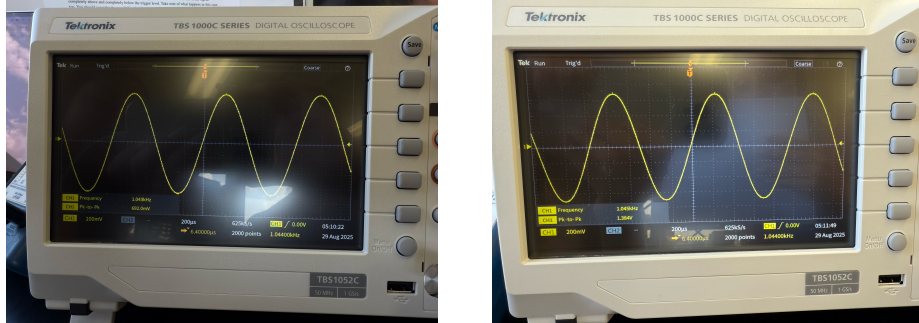


Figure 2: Oscilloscope display of a 1 kHz sine wave with (left) and without (right) a 50Ω terminator.

Without the terminator connected, the oscilloscope's input impedance (approximately $1\text{M}\Omega$) is much larger than the source impedance, so close to the full open-circuit voltage appears at the input and causes a higher amplitude. The frequency and shape of the waveform stay constant, which confirms that the oscilloscope measures voltage rather than current and functions as a voltmeter, not an ammeter.



Figure 3: Circuit schematics of the function generator and oscilloscope connection with (left) and without (right) a 50Ω terminator.

2.4.2 Scope triggering

When we set the trigger level within the amplitude of the sine wave, the oscilloscope locked onto a consistent crossing point and displayed a stable waveform. However, when we moved the trigger level outside the signal's range, the scope was unable to synchronize to a valid trigger, thus resulting in an unstable waveform.

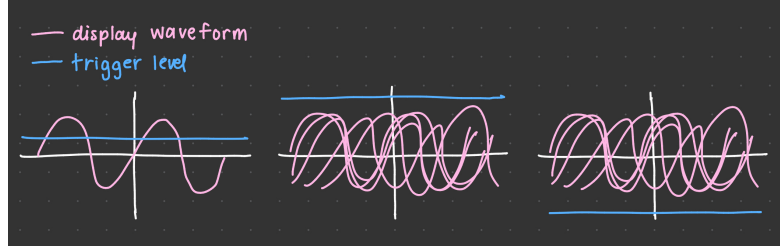


Figure 4: Sketch of oscilloscope traces showing a stable sine wave when the trigger level is within the signal range (left) and unstable displays when the trigger level is set above or below the waveform (middle and right).

When we switched the trigger source to the TTL output of the function generator, the sine remained stable as we adjusted the trigger level up and down. Even when the DC offset shifted the waveform above or below the trigger level, the display did not become unstable. The advantage of TTL triggering is that it provides a well-defined and consistent timing reference that is independent of the waveform's amplitude or offset.

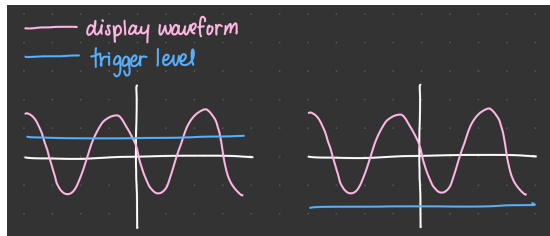


Figure 5: Sketch of sine wave in CH1 remaining stable when triggered on the TTL output of the function generator (CH2).

2.4.3 Square wave

With DC coupling, changing the DC offset shifted the entire square wave either up or down relative to ground. With AC coupling, the DC component was blocked and the waveform was centered around 0V regardless of offset. The resulting scope display is shown in Figure 6.

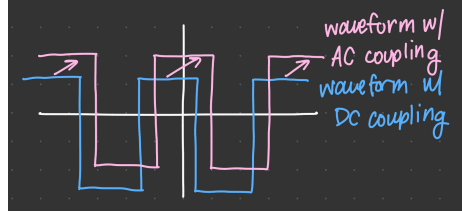


Figure 6: Sketch of oscilloscope display for a square wave with DC offset (shown in DC coupling) and AC coupling.

2.4.4 Function generator output impedance

We modeled the function generator as a source with an internal resistance R_{out} in series with its output. By attaching different load resistors R_{Load} , we measured the corresponding V_{out} . The circuit behaves like a voltage divider, described by the equation:

$$V_{\text{out}} = V \frac{R_{\text{Load}}}{R_{\text{out}} + R_{\text{Load}}} \quad (4)$$

Rearranging this into a linear form gives:

$$\frac{1}{V_{\text{out}}} = \frac{1}{V} + \frac{R_{\text{out}}}{V} \left(\frac{1}{R_{\text{Load}}} \right) \quad (5)$$

Plotting $1/V_{\text{out}}$ versus $1/R_{\text{Load}}$ produced a straight line, as shown in Figure 7. The y-intercept corresponds to $1/V$, and the slope corresponds to R_{out}/V . Using these values, we calculated the open-circuit voltage and the internal output resistance of the function generator with the formulas:

$$V = \frac{1}{\text{intercept}} \quad (6)$$

$$R_{\text{out}} = \frac{\text{slope}}{\text{intercept}} \quad (7)$$

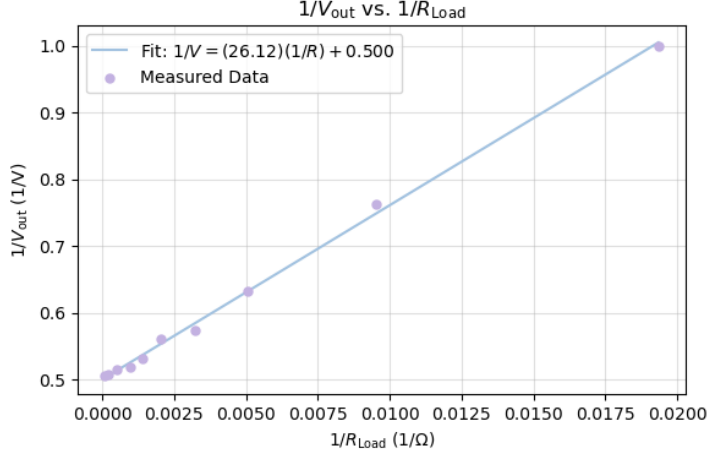


Figure 7: Plot of $1/V_{\text{out}}$ vs. $1/R_{\text{load}}$ showing a linear relationship consistent with the voltage divider model.

We used ten load resistors ranging from approximately 50Ω to $10k\Omega$. As expected, the V_{out} increased with increasing R_{Load} , and the plot displayed a clear linear trend consistent with theory. The values we extracted, $V = 1.99\text{V}$ and $R_{\text{out}} = 52.2\Omega$, agree within reason with the nominal 50Ω output impedance of the function generator. Minor deviations likely came from resistor tolerances, cable losses, and oscilloscope measurement error.

2.4.5 RMS amplitude

We used a DMM in AC mode to measure the RMS amplitude of sine, triangle, and square waveforms at 10Hz, 1kHz, and 100kHz, each with a peak-to-peak voltage of 2V and zero DC offset. The theoretical RMS values for a $2V_{\text{pp}}$ waveform are:

- Sine wave: 0.707 V
- Triangle wave: 0.577 V
- Square wave: 1.000 V

Our measurements are summarized in Table 1 below. At low frequencies (10Hz), the DMM significantly under-reported values for the sine and triangle waves, which is likely due to its limited AC bandwidth or the internal coupling capacitor not passing low-frequency signals effectively. At higher frequencies (10Hz and 100kHz), our measurements approached theoretical values, especially for the square wave.

Frequency	Sine	Triangle	Square
10 Hz	0.100 V	0.120 V	2.000 V
1 kHz	1.980 V	1.900 V	2.020 V
100 kHz	2.060 V	1.920 V	2.040 V

Table 1: Measured RMS amplitudes of sine, triangle, and square waves at different frequencies (2 Vpp input).

2.4.6 Rise time

We set the function generator to produce a 1MHz square wave and measured the rise time using the oscilloscope's automatic measurement function. The rise time, defined as the time it takes for the signal to rise from 10% to 90% of its peak value, was 62.7ns. This nonzero value reflects the bandwidth of the function generator and oscilloscope, which constrains how sharply we can reproduce signal transistions.

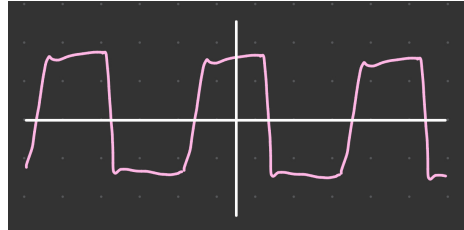


Figure 8: Sketch of observed oscilloscope waveform for a 1MHz square wave.

3 Lab 2: RC Circuits

3.1 Circuit A

3.1.1 Rise and fall time

Figure 9 shows the output waveform of Circuit A. We measured the time constants for the rising and falling edges as 480 μ s. The resistor and capacitor measured with the DMM were $R = 20.11\text{k}\Omega$ and $C = 5.48\text{nF}$, giving a theoretical time constant of $\tau = RC = 110\text{\mu s}$. Thus, the time constant we observed was larger than expected, likely due to non-ideal component tolerances and oscilloscope input loading.

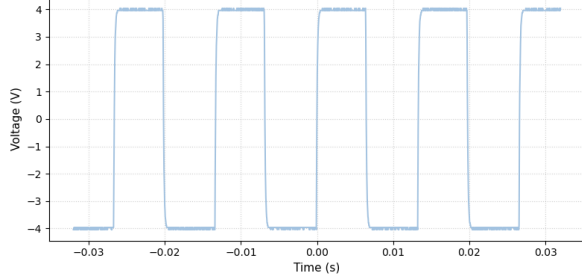


Figure 9: Output waveform showing the exponential rise and fall of Circuit A.

3.1.2 Integrator

Figure 10 shows the output waveforms of Circuit A at various frequencies. Although we were not able to get a clear square wave shape at the lowest frequency, as we increased the frequency, the output transitioned to a more smooth triangular waveform. At low frequencies, the capacitor charged and discharged more fully, so the output more closely follows the input. At higher frequencies, each half-cycle becomes shorter, causing the capacitor to charge for less time and reduces the peak-to-peak amplitude of the output.

This behavior is consistent with the expected integrator relation:

$$V_{\text{out}}(t) = V_{\text{out}}(0) + \frac{1}{RC} \int_0^t V_{\text{in}}(t') dt', \quad (8)$$

for $\omega \gg \frac{1}{RC}$, which confirms that Circuit A indeed functions as an integrator.

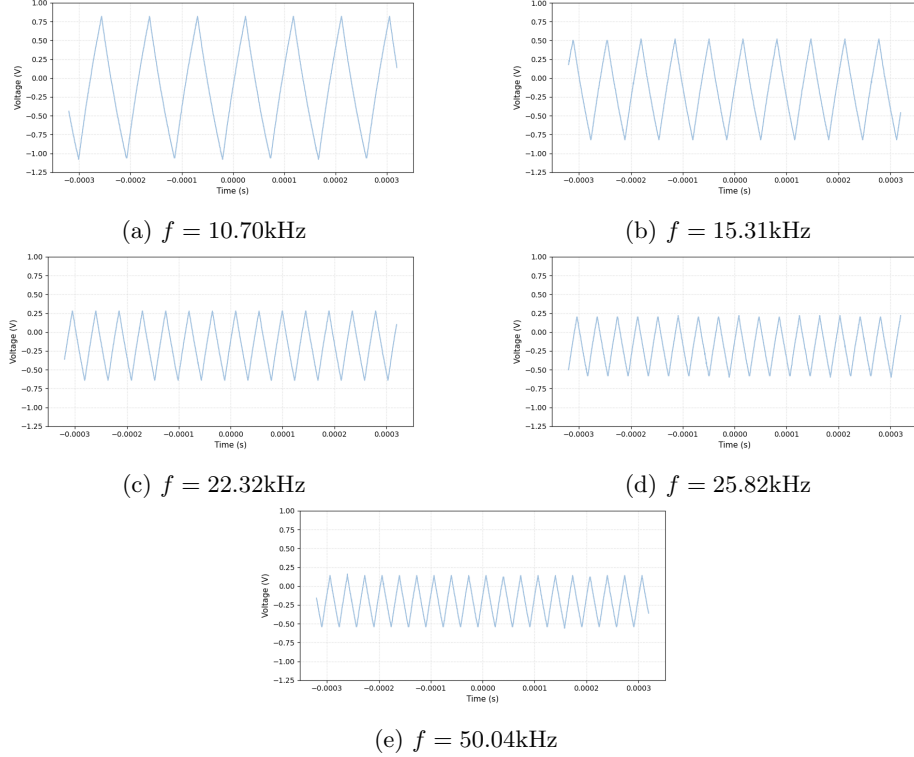


Figure 10: Output voltage of Circuit A at increasing input frequencies.

3.1.3 Low-pass filter

Next, we tested the frequency response of low-pass filter Circuit A by measuring the gain and phase shift over a range of frequencies spanning well above and below the theoretical cutoff frequency. Figure 12 shows the gain plot exhibiting low-pass behavior, with the 3dB point occurring near the expected cutoff frequency of a little over 1kHz. Figure 13 shows the phase becoming increasingly negative with frequency, which aligns with low-pass filter theory.

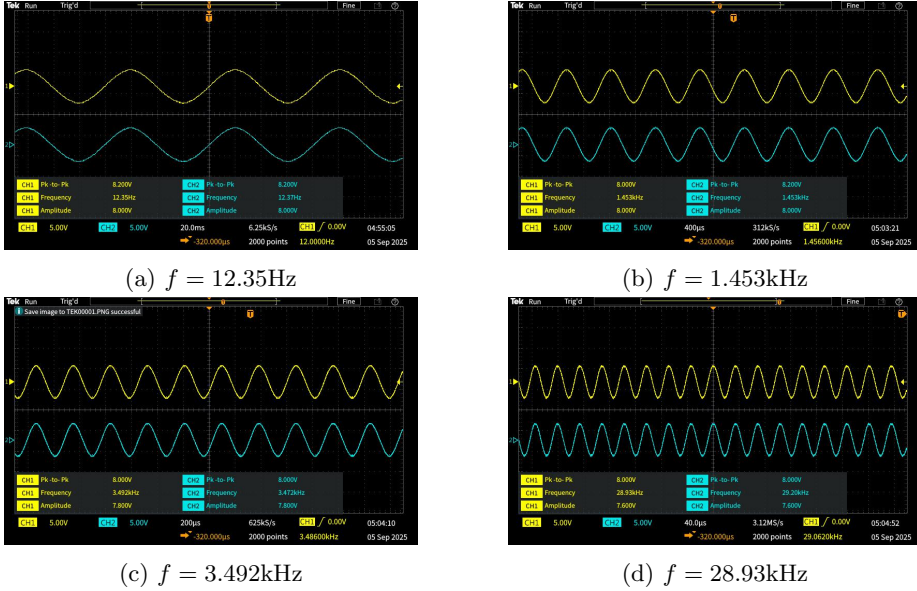


Figure 11: Representative scope displays for low-pass filter Circuit A at varying frequencies.

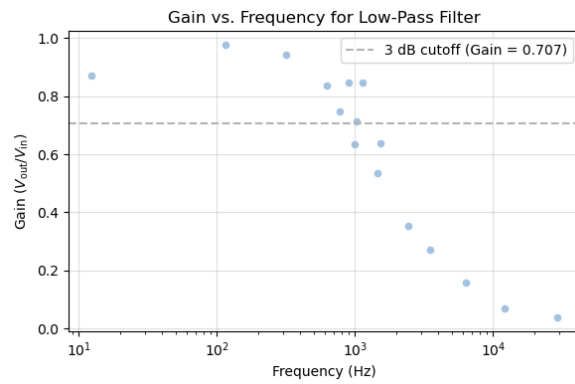


Figure 12: Gain vs. frequency for the low-pass filter Circuit A.

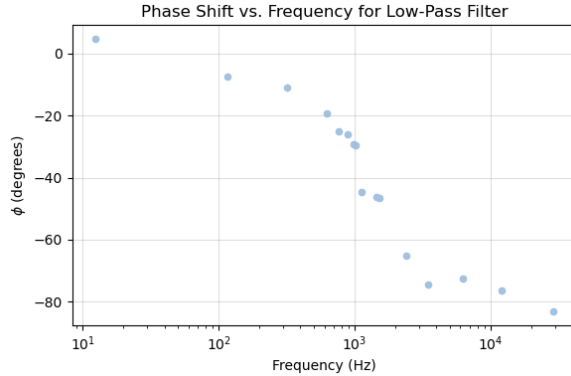


Figure 13: Phase shift vs. frequency for the low-pass filter..

3.2 Circuit B

3.2.1 Time constants

We drove circuit B with a square wave (no DC offset) to observe exponential decays during each transition. A copy of the waveform is shown in Figure 14.

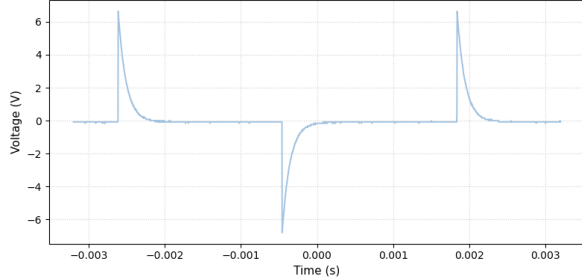


Figure 14: Output waveform showing the the exponential decays for Circuit B.

From the oscilloscope, we measured the positive decay time constant as $340\mu\text{s}$ and the negative time decay constant as $444\mu\text{s}$. The measurements differ slightly, which is likely due to measurement error or asymmetries in the circuit. The theoretical time constant is $\tau = RC = 110\mu\text{s}$. Our measurements were higher but within the same order of magnitude than the predicted value, which may result from input loading or limitations in cursor placement on the oscilloscope.

3.2.2 Differentiator

We configured Circuit B as a differentiator and applied a triangle wave input at various frequencies. According to Equation (2.2):

$$V_{\text{out}} = RC \frac{dV_{\text{in}}}{dt}, \quad (9)$$

the output should approximate the derivative of the input waveform when the driving frequency satisfies $\omega \ll \frac{1}{RC}$.

As shown in Figure 15, at high frequencies, the output follows the triangular input, which indicates the circuit is not acting as a differentiator. As we decreased the frequency, the waveform started to resemble a square wave, which is the expected derivative of a triangle wave since triangle slopes are constant. The lowest frequency we tested was 196.9Hz. At this value, the output approximates an ideal square wave, which confirms expected differentiator behavior.

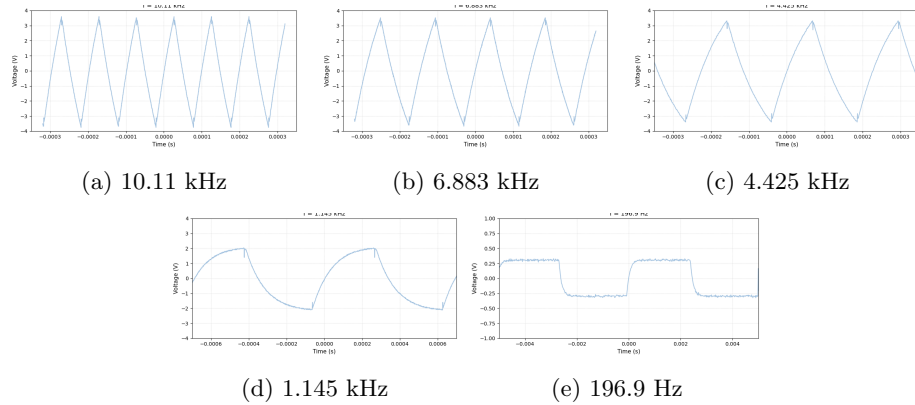


Figure 15: Output waveforms of the RC differentiator circuit at various input triangle wave frequencies.

3.2.3 High-pass filter

Next, we measured the gain and phase of high-pass filter Circuit B as a function of frequency. Scope traces at four different frequencies are included in Figure 16, showing how the output signal evolves along with frequency.

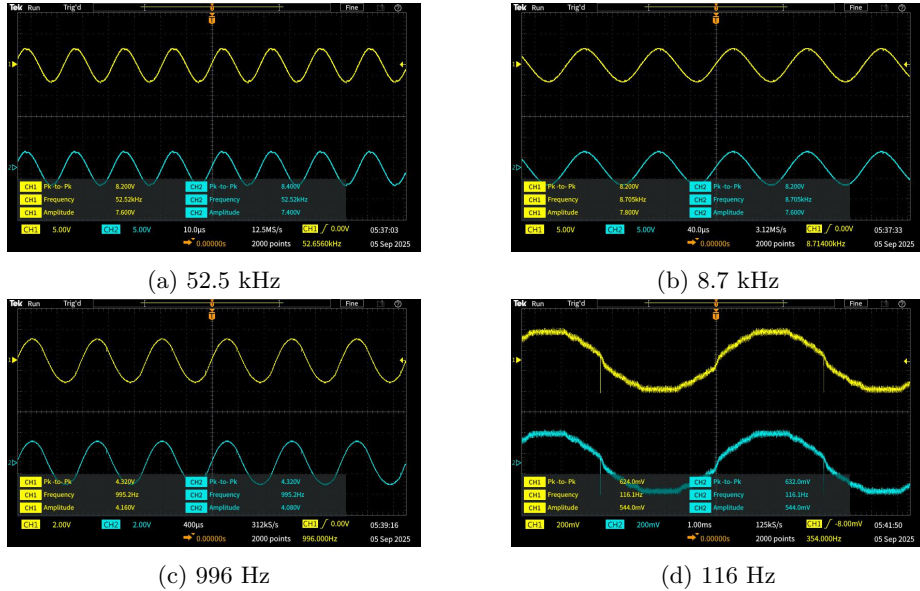


Figure 16: Oscilloscope displays of input (CH1) and output (CH2) voltages for the high-pass filter at various drive frequencies.

The gain curve in figure 17 shows that the filter passes high frequencies while suppressing low ones, as expected. The 3dB point occurs at a little over 1kHz and marks the cutoff frequency. The phase shift plot in Figure 18 shows the transition from 90° to 0° at higher frequencies. This behavior is consistent with what is expected with a first-order high-pass filter.

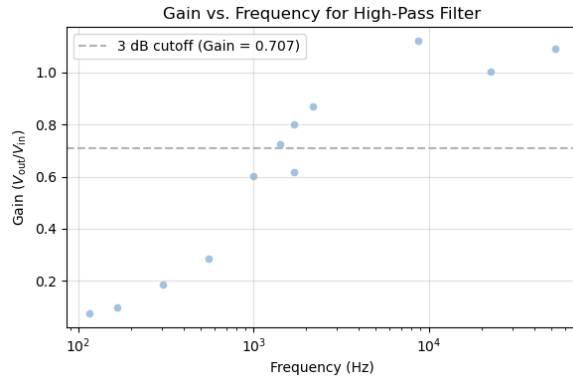


Figure 17: Gain vs. frequency for the high-pass filter.

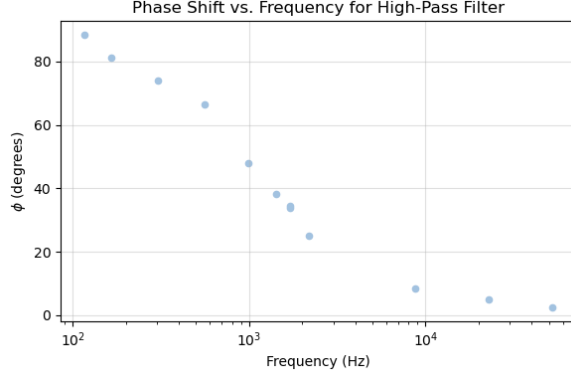


Figure 18: Phase shift vs. frequency for the high-pass filter.

3.3 Comparison with theory

3.3.1 Circuit A

To analyze the low-pass circuit A, we used the complex impedance method to derive the gain and phase shift as functions of frequency. The transfer function is:

$$\frac{V_{\text{out}}}{V_{\text{in}}} = \frac{1}{1 + j\omega RC}. \quad (10)$$

Taking the magnitude gives us the theoretical gain:

$$\left| \frac{V_{\text{out}}}{V_{\text{in}}} \right| = \frac{1}{\sqrt{1 + (\omega RC)^2}}, \quad (11)$$

which makes the phase shift:

$$\phi = -\arctan(\omega RC). \quad (12)$$

Using the values $R = 20\text{k}\Omega$ and $C = 0.005\mu\text{F}$, we plotted the theoretical gain and phase shift versus frequency. The cutoff occurs at $f_0 = \frac{1}{2\pi RC} \approx 1.6\text{kHz}$ where the gain drops to 0.707, which is the -3dB point. The phase shift transitions from 0° at low frequencies to -90° at high frequencies.

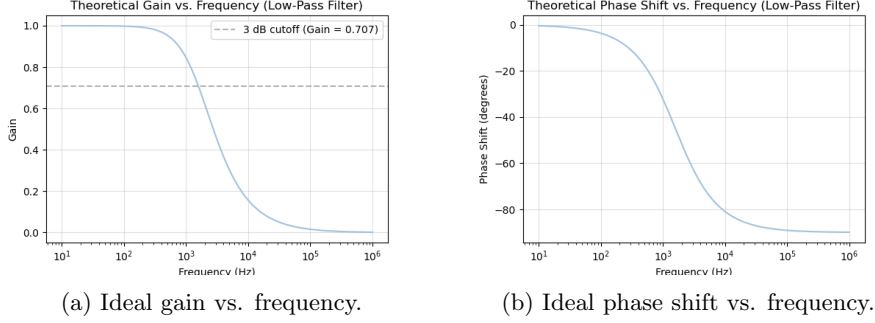


Figure 19: Theoretical frequency responses for Circuit A (low-pass filter).

Our measured gain and phase data align well with the theory across most of the frequency range, which confirms the expected behavior of a low-pass filter. Minor discrepancies appear at higher frequencies (above 20kHz), where the gain decreases more rapidly and the phase shift begins to flatten. These likely reflect non-ideal effects such capacitor ESR or parasitic inductance, which become more pronounced at high frequencies. Overall.

3.3.2 Circuit B

To analyze the high-pass Circuit B, we used the complex impedance method to derive the gain and phase shift as functions of frequency. The transfer function is:

$$\frac{V_{\text{out}}}{V_{\text{in}}} = \frac{j\omega RC}{1 + j\omega RC}. \quad (13)$$

Taking the magnitude gives us the theoretical gain:

$$\left| \frac{V_{\text{out}}}{V_{\text{in}}} \right| = \frac{\omega RC}{\sqrt{1 + (\omega RC)^2}}. \quad (14)$$

which makes the phase shift:

$$\phi = 90^\circ - \arctan(\omega RC). \quad (15)$$

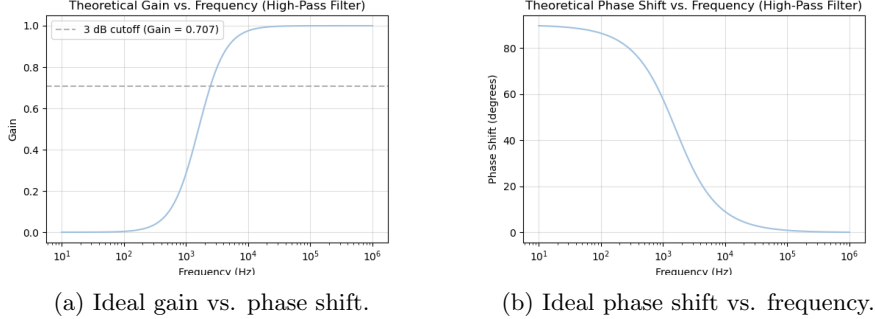


Figure 20: Theoretical frequency responses for Circuit B (high-pass filter).

Our theoretical plots of gain and phase versus frequency confirm the expected high-pass filter behavior where gain approaches zero at low frequencies and approaches 1 at high frequencies. The phase starts near -90° and approaches 0° as frequency increases.

Our measured data agrees with the theoretical models. The 3dB point occurs at the cutoff frequency ($\approx 1.6\text{kHz}$), and both plots generally follow the predicted trend, though we observed minor deviations due to experimental noise or oscilloscope resolution limits. Overall, our measurements confirm the behavior of an ideal high-pass filter.

4 Lab 3: Inductors and LC Filter Circuits

4.1 Impedance measurement with the LCR meter

We used a Bourns RL181S-102J-RC inductor to observe how its impedance characteristics change with frequency. We measured the inductor's properties at four different frequencies (100 Hz, 1 kHz, 10 kHz, and 100 kHz) using an LCR meter. We obtained the series inductance L_S , quality factor Q , equivalent series resistance (ESR), and phase angle θ . The results are summarized in Table 2.

Frequency	L_S (μH)	Q	ESR (Ω)	θ (deg)
100 Hz	950.0	0.274	2.1	15.3
1 kHz	944.4	2.69	2.2	69.6
10 kHz	944.6	23.7	2.5	87.5
100 kHz	928.5	137.0	4.12	89.5

Table 2: Measured inductor parameters (Bourns RL181S-102J-RC) at various frequencies.

According to the manufacturer's datasheet, the inductor has a nominal inductance of 1000 μH with a tolerance of $\pm 5\%$, a minimum quality factor $Q = 70$

at 50 kHz, and a self-resonant frequency (SRF) of 0.77 MHz. Our measured inductance values ranged from 928.5 μ H to 950.0 μ H, which are well within our expectations.

From our measurements, we observed that at low frequencies (100 Hz), the inductor deviated significantly from ideal behavior, exhibiting a low quality factor (Q) and a small phase angle (θ). As the frequency increased, the inductor's behavior approached that of an ideal inductor. Q increased, θ approached 90°, and the ESR remained relatively low. The inductor behaved most ideally between 10 kHz and 100 kHz, where Q was high and the phase angle was nearly 90°.

To verify the consistency of ESR and Q values, we used the definition of quality factor:

$$Q = \frac{\omega L_s}{\text{ESR}}. \quad (16)$$

At $f = 1$ kHz, using $L_s = 944.4 \mu$ H and ESR = 2.2 Ω , we computed:

$$Q = \frac{2\pi(1000)(944.4 \times 10^{-6})}{2.2} \approx 2.70, \quad (17)$$

which indeed matches the measured value of $Q = 2.69$ and confirms the consistency of our data.

We also measured the impedance characteristics of a 100 nF ceramic capacitor using the same LCR meter across the same set of frequencies. The results are summarized in Table 3.

Frequency	C_S (nF)	D	ESR (Ω)	θ (deg)
100 Hz	99.37	0.000	n/a	-90.0
1 kHz	99.33	0.000	0.20	-90.0
10 kHz	99.28	0.000	0.06	-90.0
100 kHz	99.31	0.001	0.02	-90.0

Table 3: Measured parameters for 100nF ceramic capacitor at various frequencies.

Across all frequencies, the measured capacitance remained consistent around 99.3 nF. The phase angle θ also stayed consistently at -90°, suggesting nearly ideal capacitive behavior. The dissipation factor D remained extremely low and the equivalent series resistance (ESR) decreased with increasing frequency, which is what we expected.

Comparing both components, the ceramic capacitor exhibited behavior much closer to an ideal capacitor than the inductor did to an ideal inductor. Its phase angle stayed the same at -90° and the ESR was minimal across the entire frequency range. The dissipation factor D being close to 0 also indicates that nearly all the energy is stored and returned rather than dissipated as heat.

The inductor, on the other hand, only approached ideal behavior at higher frequencies (10kHz and above).

4.2 Impedance measurements with an oscilloscope

We used the oscilloscope to measure the voltage across the inductor (CH1), the voltage across the series resistor (MATH), and the phase difference between them. Although we intended to measure at 1kHz, the signal generator was inadvertently set to 25.42kHz and the waveform somewhat unstable. We performed our analysis based on this actual frequency.

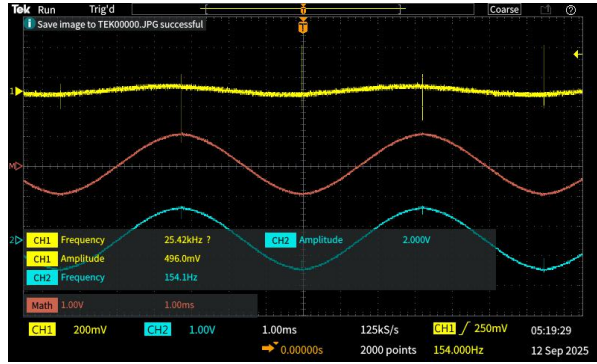


Figure 21: Oscilloscope display showing voltage across the inductor (CH1), voltage across the resistor(MATH).

The voltage across the inductor was 496mV, and the voltage across the resistor was 1.00V, giving us a current of 10mA. Using the relation $L_S = V_L/(\omega I)$ and $\omega = 2\pi f = 159719\text{rad/s}$, we calculated:

$$L_S = \frac{0.496}{159719 \cdot 0.01} \approx 311\mu\text{H}. \quad (18)$$

This value is significantly lower than the LCR measurement at 1kHz (944 μH), likely due to frequency dependence and limitations in the CH1 measurement. We calculated the ESR as $V_R/I = 100\Omega$ and the quality factor as:

$$Q = \frac{\omega L_S}{\text{ESR}} \approx 0.50. \quad (19)$$

We estimated the phase angle visually using the oscilloscope and approximated the time offset between the CH1 and MATH waveforms as 7.1 μs . With a waveform period of $T = 1/f \approx 39.3\mu\text{s}$, this corresponds to:

$$\theta \approx 360^\circ \cdot \frac{7.1}{39.3} \approx 64^\circ. \quad (20)$$

The current we measured of 10mA is well below the rated maximum of 90mA, which confirms the component was not approaching saturation or overheating

during measurement.

Finally, we went through input frequencies from 50kHz to 1MHz and observed resonance behavior near 770kHz. This agrees with the inductor's specified SRF of 0.77MHz. Beyond this point, the inductor exhibits capacitive behavior.

4.3 Notch filter

Next, we built a notch filter RLC circuit using a 1mH inductor and a 4.7nF capacitor. We measured the gain $|\tilde{V}_{\text{out}}/\tilde{V}_{\text{in}}|$ across a range of frequencies and plotted it in Figure 22. As expected for a series notch filter, the gain goes through a sharp dip near the resonant frequency since this is where the voltage drops due to impedance cancellation between the inductor and capacitor.

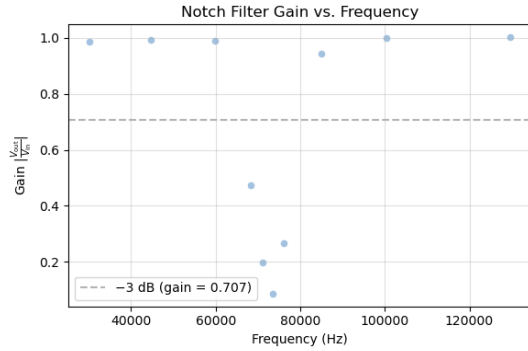


Figure 22: Gain vs. frequency for the notch filter circuit.

From the plot, we observed the minimum gain occurs at approximately $f_0 \approx 73.2\text{kHz}$, where $|\tilde{V}_{\text{out}}/\tilde{V}_{\text{in}}| \approx 0.084$. We visually estimated the -3dB points to be 68kHz and 81kHz, giving us a bandwidth of approximately 13.0kHz. We calculated the experimental quality factor:

$$Q = \frac{f_0}{\text{bandwidth}} = \frac{73.2\text{kHz}}{13.0\text{kHz}} \approx 5.63. \quad (21)$$

Next, we find the equivalent series resistance to reach this quality factor:

$$R = \frac{1}{Q} \sqrt{\frac{L}{C}} \approx 81.9\Omega. \quad (22)$$

This value corresponds to the total resistance in the inductor and circuit wiring. The relatively sharp notch and moderate Q suggest reasonable energy loss and confirm the expected series RLC behavior.

Our theoretical predictions also align with our measured values. Using $L = 1\text{mH}$ and $C = 4.7\text{nF}$, we calculate the resonant frequency:

$$f_0 = \frac{1}{2\pi\sqrt{LC}} \approx 73.3\text{kHz}, \quad (23)$$

which is close to our observed value of $f_0 \approx 73.2\text{kHz}$. Thus, we confirm our notch filter setup behaves as expected in theory.

4.4 Second-order Butterworth filter

Finally, we constructed a second-order Butterworth filter using a 1mH inductor and a 4.47nF capacitor, which gives us a resonant (cutoff) frequency of approximately 73.3kHz . From the formula for an ideal Butterworth filter:

$$R = \frac{1}{2\sqrt{2}\pi f_0 C}, \quad (24)$$

we found the required resistor value to be about 343.5Ω . We used three 100Ω resistors in series to give us a total resistance of roughly 300Ω during our experiment.

We measured $|\tilde{V}_{\text{out}}/\tilde{V}_{\text{in}}|$ at various frequencies and plotted the our data on a log-log scale. The curve shows the gain close to 1 at low frequencies, then begins to decrease beyond the resonant (cutoff) frequency, which is expected behavior of a second-order Butterworth filter.

At high frequencies, the gain should fall off as $1/f^2$, which corresponds to a slope of -40dB per order in a log-log plot. Our data generally follows the expected slope in the high-frequency region, which confirms that our filter behaves as predicted. Minor deviations are likely due to component tolerances or limitations in the measurement setup.

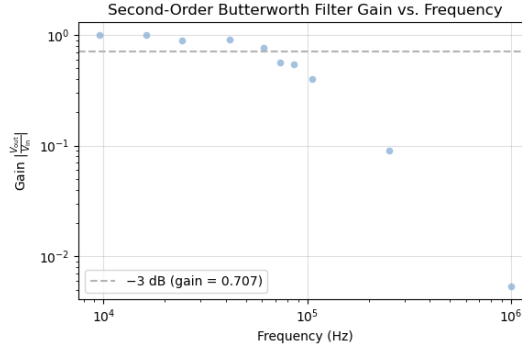


Figure 23: Gain vs. frequency on a log-log scale for the second-order Butterworth filter.

Acknowledgements

We would like to thank our laboratory instructor, Dr. Heinzen, and our teaching assistant, Kyle Gable, for their guidance and support through these labs. Their assistance and feedback were invaluable in helping us understand the experimental procedures and circuit concepts. We also appreciate the department's laboratory facilities and equipment, which made these experiments possible.